



# Kent Academic Repository

Dixey, Richard J. C., Wildes, Andrew, Doheny, Patrick W., Stenning, Gavin B. G. and Saines, Paul J. (2023) *The magnetocaloric effect of the lanthanide fluorides: Using polarized neutron scattering to probe a magnetocaloric suitable for hydrogen liquefaction*. *APL Materials*, 11 (4). ISSN 2166-532X.

## Downloaded from

<https://kar.kent.ac.uk/101044/> The University of Kent's Academic Repository KAR

## The version of record is available from

<https://doi.org/10.1063/5.0139726>

## This document version

Author's Accepted Manuscript

## DOI for this version

## Licence for this version

UNSPECIFIED

## Additional information

For the purpose of open access, the author has applied a CC BY public copyright licence (where permitted by UKRI, an Open Government Licence or CC BY ND public copyright licence may be used instead) to any Author Accepted Manuscript version arising.

## Versions of research works

### Versions of Record

If this version is the version of record, it is the same as the published version available on the publisher's web site. Cite as the published version.

### Author Accepted Manuscripts

If this document is identified as the Author Accepted Manuscript it is the version after peer review but before type setting, copy editing or publisher branding. Cite as Surname, Initial. (Year) 'Title of article'. To be published in ***Title of Journal***, Volume and issue numbers [peer-reviewed accepted version]. Available at: DOI or URL (Accessed: date).

## Enquiries

If you have questions about this document contact [ResearchSupport@kent.ac.uk](mailto:ResearchSupport@kent.ac.uk). Please include the URL of the record in KAR. If you believe that your, or a third party's rights have been compromised through this document please see our [Take Down policy](https://www.kent.ac.uk/guides/kar-the-kent-academic-repository#policies) (available from <https://www.kent.ac.uk/guides/kar-the-kent-academic-repository#policies>).

# The Magnetocaloric Effect of the Lanthanide Fluorides: Using Polarised Neutron Scattering to Probe a Magnetocaloric Suitable for Hydrogen Liquefaction

Richard J. C. Dixey<sup>1</sup>, Andrew Wildes<sup>2</sup>, Patrick W. Doherty<sup>3</sup>, Gavin B. G. Stenning<sup>4</sup> and Paul J. Saines<sup>\*3</sup>

<sup>1</sup>Centre for Condensed Matter, Queen Mary University of London, London, E1 4NS, UK

<sup>2</sup>Institut Laue-Langevin, CS 20156, 38042 Grenoble Cedex 9, France

<sup>3</sup>School of Chemistry and Forensic Science, Ingram Building, University of Kent, Canterbury, CT2 7NH, UK

<sup>4</sup>ISIS Facility, STFC Rutherford Appleton Laboratory, Chilton, Didcot, OX11 0QX, United Kingdom

This work reports the competitive magnetocaloric effect of some simple lanthanide fluoride materials with cations with high magnetic anisotropy. Of these HoF<sub>3</sub> is particularly promising due to exhibiting a high magnetocaloric entropy change under modest applied fields at higher temperatures, which only decreases modestly with temperature such that it has potential for cooling for hydrogen liquifaction. Spin polarised neutron spectroscopy indicates its promising conventional magnetocaloric effect is likely due to the presence of ferromagnetic fluctuations of highly anisotropic magnetic moments while its singlet electronic ground state and low temperature magnetic ordering leads to a decrease in its magnetocaloric performance below 4 K.

## I. Introduction

The magnetocaloric effect (MCE) is an energy-efficient and environmentally friendly alternative to vapour compression refrigeration technology, with superior theoretical energy efficiencies of >50 % compared to ~35% for vapour compression.<sup>1,2</sup> Whilst magnetocalorics have historically been optimised for ultra-low temperature (< 2 K), they have recently been considered suitable as a replacement for liquid helium refrigeration or liquefaction of hydrogen gas (< 20 K) as promising MCE at higher temperatures is achieved.<sup>3,4</sup> The MCE arises from the change in entropy when a magnetic field is applied and then removed from a paramagnetic material. Initial application of a magnetic field causes the spins to align with the external magnetic field, to produce a more ordered state thereby reducing the magnetic entropy of the system. This results in a positive adiabatic temperature change ( $\Delta T_{ad}$ ) as the total magnetic entropy of the system approaches 0. If this heat subsequently removed from the system whilst the field is still applied, when the field is removed the entropy of the system increases and a negative  $-\Delta T_{ad}$  results. This cooling process can be iterated to lower the temperature of the material, but for this effect to work optimally the material must remain paramagnetic over the working temperature range

The need for dense magnetocalorics with high magnetic moments has driven an interest in MCE materials based on the later lanthanides because of the high magnetic entropy change ( $\Delta S_m$ ), they support. A new wave of non-oxide magnetocalorics have been recently reported to have particularly high magnetocaloric effects, including Gd(HCO<sub>2</sub>)<sub>3</sub>(C<sub>2</sub>O<sub>4</sub>), GdPO<sub>4</sub>, Gd(HCO<sub>2</sub>)<sub>3</sub>, GdOHCO<sub>3</sub> and GdF<sub>3</sub>, which have superior performance to the benchmark Gd<sub>3</sub>Ga<sub>5</sub>O<sub>12</sub> (GGG) phase.<sup>5-10</sup> Recent work has shown the substitution of Gd for other lanthanide ions with Ising-like spins leading to larger  $-\Delta S_m$  above 2 K in low applied fields,<sup>11-14</sup> at the expense of some decrease of performance for larger field changes. Achieving magnetocaloric materials optimised for higher temperatures and, ideally, the

more modest applied fields that can be generated using a permanent magnet (less than 2 T) offers the potential high efficiency cryogen-free cooling technology for a wider range of applications. This has inspired the study of analogues of promising Gd magnetocalorics containing other, magnetically anisotropic, lanthanides.

The benefits of exploring magnetocalorics with magnetically anisotropic cations has already been highlighted by studies of the  $Ln(\text{HCO}_2)_3$  ( $Ln = \text{Gd}^{3+}, \text{Tb}^{3+}, \text{Dy}^{3+}, \text{Ho}^{3+}$  and  $\text{Er}^{3+}$ ) which have shown that Tb(HCO<sub>2</sub>)<sub>3</sub> has higher  $-\Delta S_m$  than Gd(HCO<sub>2</sub>)<sub>3</sub> above 4 K and field changes below 2 T.<sup>11</sup> Similarly amongst the  $Ln\text{OHCO}_3$  phases TbOHCO<sub>3</sub> and DyOHCO<sub>3</sub> have higher  $-\Delta S_m$  than GdOHCO<sub>3</sub> above 4 K for similarly modest field changes.<sup>12</sup> Previous studies of these two families have shown that the reason these materials are able to stay paramagnetic in their magnetocaloric operating temperatures due to significant frustration between neighbouring chains of spins which are arranged in triangular motifs, stacked into layers forming chains of magnetic ions.<sup>11,15-18</sup> These Ising-like spin chains also possess strong intrachain ferromagnetic correlations which allow for easy alignment of the spins with the magnetic fields once the antiferromagnetic correlations are overcome.

The  $LnF_3$  family of materials crystallise in the orthorhombic  $Pnma$  space group ( $a = 6.40$ ,  $b = 6.87$  and  $c = 4.38$  Å for HoF<sub>3</sub> at room temperature).<sup>19</sup> The structure can be viewed as having chains of  $LnF_9$  face-sharing polyhedra, with corner-sharing interchain connectivity. Intrachain nearest neighbour Ho<sup>3+</sup> are separated by 3.6 Å, with the next nearest neighbour interchain distance of 4.1 Å. The  $LnF_3$  phases have similar structural characteristics to the  $Ln(\text{HCO}_2)_3$  and  $Ln\text{OHCO}_3$  phases with their chains packed into distorted triangular lattices (see **FIG. 1**) GdF<sub>3</sub> is reported to have the highest  $-\Delta S_m^{\text{max}}$  and we have, therefore chosen to investigate the magnetocaloric effect in the  $LnF_3$  family of materials.<sup>8</sup> We find that HoF<sub>3</sub> has significantly higher  $-\Delta S_m$  than GdF<sub>3</sub> at low fields above 4 K, with a slow decrease in performance being particularly impressive enabling it to retain high  $-\Delta S_m$  well above 10 K. This makes it useful for cooling over

a significantly broader range of temperatures, and therefore applications, than is typical for a magnetocaloric, including cooling to near 20 K for hydrogen liquefaction. Below 4 K the  $-\Delta S_m$  of  $\text{HoF}_3$  decreases significantly, leading to apparent inverse MCE at 2 K. This is attributed to a combination of its, previously reported, singlet electronic ground state and low temperature canted antiferromagnetic order.<sup>20,21</sup>

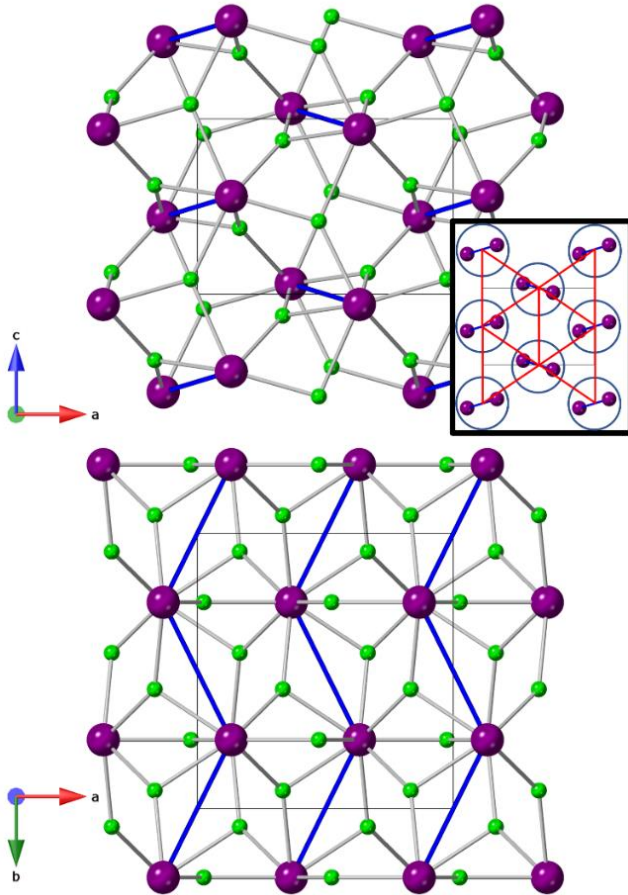


**FIG. 1:** Two diagrams of the isostructural  $\text{LnF}_3$  materials, oriented along the  $b$  and  $c$  axes.  $\text{Ln}^{3+}$  are shown in purple, and F are shown in green. Nearest neighbour interactions are shown as blue rods. The top diagram oriented along the  $b$ -axis shows the triangular motifs in the insert, between buckled spin chains, and the bottom diagram shows the nearest neighbour interactions forming chains of  $\text{Ln}^{3+}$  atoms. Crystal structure data taken from M. Piotrowski *et al.*<sup>19</sup>

## II. Experimental Methods

Polycrystalline samples of  $\text{LnF}_3$  ( $\text{Ln} = \text{Gd}^{3+}, \text{Tb}^{3+}, \text{Dy}^{3+}, \text{Ho}^{3+}$  and  $\text{Er}^{3+}$ ) were purchased from Fisher Scientific without any further purification. Sample phase purity was examined by powder X-ray diffraction measurements performed on ground polycrystalline samples on a Rigaku MiniFlex with  $\text{CuK}\alpha$  radiation with the use of a zero-background silicon sample holder. X-ray patterns were refined using the FULLPROF suite using the Pawley fitting method, and a linear background of interpolated points (see **FIG. S1-5** for the resulting fits), which indicated that only  $\text{DyF}_3$  contained a small unknown impurity.<sup>22</sup>

The magnetic measurements of the polycrystalline samples (15-20 mg) were performed using a Quantum Design MPMS

SQUID magnetometer. Samples were placed in gelatine capsules enclosed inside a pierced straw with a uniform diamagnetic background. Zero field cooled (ZFC) and field cooled (FC) measurements were recorded in a DC field 2-300 K for  $\text{LnF}_3$  (where  $\text{Ln} = \text{Gd-Er}$ ) in 1000 Oe field. Field sweeps used to calculate  $\Delta S_m$  using Maxwell relations were measured in a DC field and fields 0-5 T, with varying intervals.

Powder neutron scattering measurements were carried out on the D7 diffuse scattering spectrometer in both diffraction and inelastic modes, at the Institut Laue-Langevin neutron reactor source in Grenoble, France.<sup>23</sup> 7.977g of polycrystalline  $\text{HoF}_3$  was ground in a pestle and mortar and loaded into an aluminium can. The can had a 20 mm inner diameter with a 19 mm insert to give the sample an annular cross-section. The experiment used polarised neutrons with a wavelength of 3.1327 Å (incident energy = 8.34 meV) from the pyrolytic graphite (002) monochromator. The neutrons were polarised and analysed using supermirror benders, with a precession-coil spin flipper in the incident beam and current-carrying coils around the sample to control the polarisation direction. The XYZ polarisation analysis method, involving the linear combinations of the measured non-spin-flip and spin-flip intensities for the polarisation along three orthogonal directions,<sup>23</sup> was used to separate out the nuclear coherent, nuclear spin-incoherent, and magnetic scattering signals from the total scattering. Diffraction measurements were carried out between 1.5 K to 150 K. A Fermi chopper was then placed between the monochromator and sample for spectroscopy measurements at 1.5 K, permitting the final neutron energy to be determined from the time-of-flight between the sample and the detectors.

## III. Results and Discussion

### A. Magnetic Properties

Field cooled (FC) and zero-field cooled (ZFC) magnetic susceptibility data of the  $\text{LnF}_3$  frameworks ( $\text{Ln} = \text{Gd}^{3+}, \text{Tb}^{3+}, \text{Dy}^{3+}, \text{Ho}^{3+}$  and  $\text{Er}^{3+}$ ) were measured in a 1000 Oe field from 2 K to 300 K. The magnetic susceptibility data for all  $\text{LnF}_3$  were found to obey Curie-Weiss law between 100 - 300 K (**FIG S6-10**). Effective magnetic moments were found to be broadly consistent with the values expected for these trivalent lanthanides according to the Russell-Saunders coupling scheme<sup>24</sup> (see **Table I**). The Curie-Weiss temperatures of  $\text{Ln} = \text{Tb-Er}$  indicates predominantly antiferromagnetic interactions within these materials, although this must be interpreted carefully due to likely contributions from crystal field effects of the  $\text{Ln}$  cations at low temperatures.

Extrapolation of the Curie-Weiss fits above 100 K to lower temperatures for  $\text{GdF}_3, \text{DyF}_3, \text{HoF}_3$  and  $\text{ErF}_3$  did not show any indication of deviation from purely paramagnetic behaviour down to 2 K (see **FIG S6, S8-S10**). In contrast  $\text{TbF}_3$  was found to deviate from Curie-Weiss law below 2.9 K with  $\chi_M T$  also increasingly rapidly at low temperature, with a maximum observed at  $\sim 3$  K (see **FIG S7 and S11**). A weak divergence of ZFC and FC magnetic susceptibility is also observed at this temperature and reflects the onset of this long range magnetic

order. This is in broad agreement with the onset of magnetic order reported in TbF<sub>3</sub> at ~3.97 K, consisting of canted Ising-spin magnetic order<sup>25,26</sup>

**Table I:** Curie-Weiss temperatures and effective magnetic moments for lanthanides in LnF<sub>3</sub>.

Ln	$\theta_{cw}$ (K)	Curie Constant (emu mol <sup>-1</sup> Oe <sup>-1</sup> )	Magnetic Moment ( $\mu_B$ )
Gd	0.42	7.32	7.65
Tb	-4.74	10.81	9.30
Dy	-4.69	12.79	10.11
Ho	-11.56	15.71	11.21
Er	-11.59	11.44	9.56

Isothermal magnetisation measurements on the LnF<sub>3</sub> frameworks measured at 2 K (**FIG. 2**) reveal that only GdF<sub>3</sub> has magnetisation consistent with a Heisenberg spin, approaching 7  $\mu_B$  under high applied magnetic fields. In contrast TbF<sub>3</sub>, DyF<sub>3</sub> and ErF<sub>3</sub> all show saturations values close to that of  $gJ/2$  expected for purely Ising anisotropy,<sup>27-30</sup> and materials with large spin-orbit coupling. Finally, HoF<sub>3</sub> shows a steep magnetisation in low applied fields and saturates at values close, but noticeable exceeding, the limit expected for the magnetic cations in an Ising case, which may suggest it exhibits high magnetic anisotropy deviating from purely Ising behaviour. This is analogous to the effect we have reported in DyOHCO<sub>3</sub>,<sup>17</sup> which showed the most promising  $\Delta S_m$  at elevated temperatures amongst the LnOHCO<sub>3</sub> phases.<sup>12,15,17</sup> The magnetisation of GdF<sub>3</sub>, TbF<sub>3</sub> and HoF<sub>3</sub> show a steep rise in magnetisation with all nearing plateau below 2 T. At 2 K none of this series show hysteresis in the magnetisation.

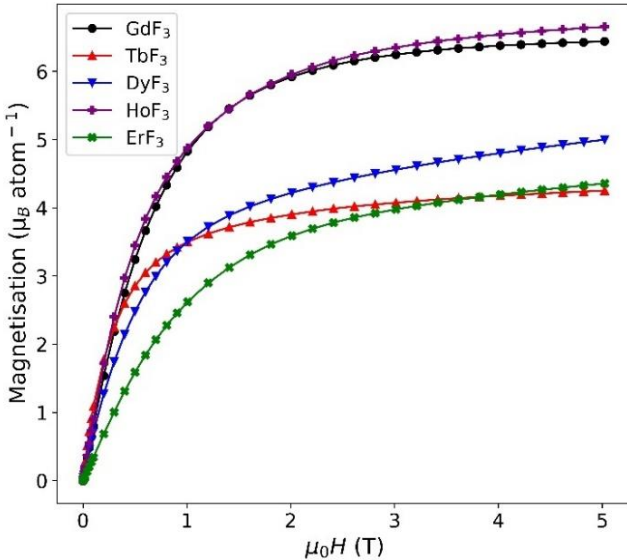


**FIG. 2:** Isothermal magnetisation measurements of the LnF<sub>3</sub>, measured at 2 K

## B. Magnetocaloric Effects

$-\Delta S_m$  were calculated using the Maxwell relation (see **Equation 1**) between 2 and 10 K, and for field changes between 0 and 1-5

T (see **FIG. 3** for 0-1 and 0-2 magnetocaloric effect plots, **FIG S12-14** for 0-3, 0-4 and 0-5 T field changes and **FIG S15-20** for magnetisation plots from which these values are obtained).

$$\Delta S_m = \int \left[ \frac{\delta M_{T, \mu_0 H}}{\delta T} \right]_{\mu_0 H} d\mu_0 H$$

**Equation 1:** The Maxwell relation used for calculating the magnetic entropy changes ( $\Delta S_m$ ) at a given temperature. Where T is absolute temperature, M is magnetisation at a given temperature and applied magnetic field, and  $\mu_0 H$  is the applied magnetic field.

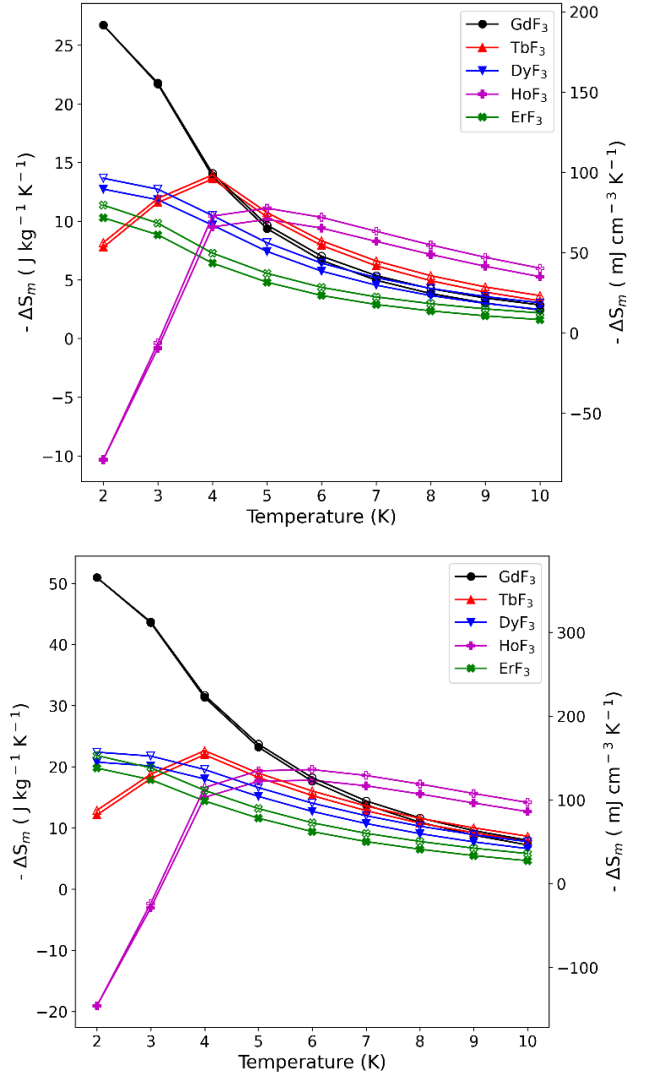


**FIG. 3:** The magnetocaloric effects of the LnF<sub>3</sub> materials in  $\Delta\mu_0 H = 0-1$  T (top) and 0-2 T (bottom). The filled and hollow symbols mark mass and volumetric units.

As expected from other lanthanide magnetocaloric materials, the previously reported GdF<sub>3</sub> is observed to have the greatest  $-\Delta S_m^{\max}$  at 2 K, particularly in multiple tesla magnetic fields. For moderate field changes of less than 2 T TbF<sub>3</sub> and HoF<sub>3</sub> are found to perform well with  $-\Delta S_m^{\max}$  at 4 K and 6 K, with HoF<sub>3</sub> outperforming GdF<sub>3</sub> above 5 K with a very gradual decrease that suggests this differential will increase significantly at higher temperatures. The slow, almost linear, decline of  $-\Delta S_m$  with respect to temperature in these initial studies inspired further

**Table II:** Summary of the peak MCE ( $-\Delta S_m^{\max}$ ) at peak temperatures ( $T_{\max}$  (K)) of the studied  $LnF_3$  at different field changes. Mass refers to changes in entropy per mass in units of  $J\ kg^{-1}\ K^{-1}$  and volume refers to change in entropy per volume in units of  $mJ\ cm^{-3}\ K^{-1}$ .

$Ln$	$\Delta\mu_0H = 0 - 1\ T$			$\Delta\mu_0H = 0 - 2\ T$			$\Delta\mu_0H = 0 - 5\ T$		
	$T_{\max}$	$\Delta S$ (Mass)	$\Delta S$ (Volume)	$T_{\max}$	$\Delta S$ (Mass)	$\Delta S$ (Volume)	$T_{\max}$	$\Delta S$ (Mass)	$\Delta S$ (Volume)
<b>Gd</b>	2	26.72	191.69	2	50.94	365.45	2	69.13	495.95
<b>Tb</b>	4	13.59	98.27	4	21.96	158.75	4	25.65	185.40
<b>Dy</b>	2	12.73	96.30	2	20.75	156.94	3	23.75	179.64
<b>Ho</b>	5	10.15	77.62	6	17.80	136.12	8	21.22	162.25
<b>Er</b>	2	10.29	79.55	2	19.78	152.89	2	25.51	197.19

investigation into the magnetocaloric effect of  $HoF_3$  to higher temperatures.

As shown in **FIG. 4** these enable the magnetocaloric entropy change for  $HoF_3$  to be calculated up to 27 K, where we observe excellent magnetocaloric behaviour, in applied fields changes of between 2 and 5 T. An anomalous reduction in the magnetocaloric effect is observed in  $HoF_3$ , in higher fields changes at 14 and 15 K. A summary of the peak MCE temperatures of all the  $LnF_3$  is given in **Table II**, showing the temperatures at which the MCE peaks in both mass and volumetric units, with regards to the performance above 4 K. Due to the high density of the  $LnF_3$  materials  $HoF_3$  outperforms other similar materials, when comparing volumetric units, above 8 K.<sup>12,16,31–33</sup>

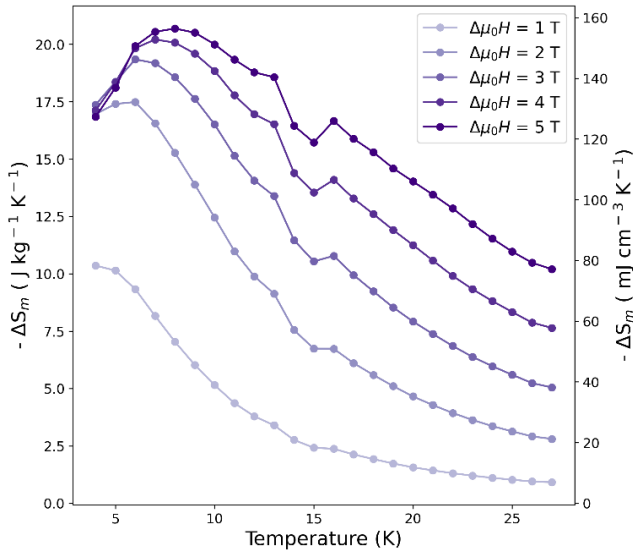


**FIG. 4:** The magnetocaloric effect of  $HoF_3$  in magnetic field changes between 1 and 5 T, plotted in mass and volumetric units.

Notably the  $-\Delta S_m$  of  $HoF_3$  decreases significantly below 4 K with an apparent inverse magnetocaloric effect at 2 K. From the Maxwell relation this can be interpreted as indicating a decrease in magnetisation with decreasing temperature ( $\delta M/\delta T$ ), as is observed in the magnetisation data. This observation should be interpreted carefully as it relies heavily on the 2 K magnetisation measurement and requires further studies to confirm this is not

an experimental artefact. If confirmed this is consistent with the material being close to a magnetic anomaly. A secondary interesting feature of  $HoF_3$ , is the field dependence of the peak temperature of the magnetocaloric effect. It appears that with larger changes in magnetic field the temperature at which the magnetocaloric effect peaks increases significantly, which has been observed in other highly anisotropic holmium containing polycrystals.<sup>34</sup>  $HoF_3$  has interesting properties compared to benchmark GGG and DGG. For  $\Delta B = 0-2\ T$  GGG has a  $-\Delta S_m^{\max} = 17.7\ J\ kg^{-1}\ K^{-1}$  or  $145\ mJ\ cm^{-3}\ K^{-1}$  at 1.2 K,<sup>33</sup> and DGG has a  $-\Delta S_m^{\max} = 11.64\ J\ kg^{-1}\ K^{-1}$  or  $95\ mJ\ cm^{-3}\ K^{-1}$  at 1.2 K,<sup>13,27,35</sup>  $HoF_3$  provides a entropy change of  $17.80\ J\ kg^{-1}\ K^{-1}$  or  $136.12\ mJ\ cm^{-3}\ K^{-1}$  at 5 K for the same field change and even at 12 and 16 K has an entropy change of greater than  $10\ J\ kg^{-1}\ K^{-1}$  or  $50\ mJ\ cm^{-3}\ K^{-1}$ , respectively.

$HoF_3$  has a  $-\Delta S_m^{\max}$  of  $21.22\ J\ kg^{-1}\ K^{-1}$  for a field change of 0-5 T and retains value of larger than  $14.02\ J\ kg^{-1}\ K^{-1}$  up to 20 K, the boiling point of hydrogen, for a 0-5 T field change. This compares favourably to the mineral Gaufreyite, which has been previously touted for use as a magnetocaloric for hydrogen liquefaction based on a  $-\Delta S_m^{\max}$  of less than  $15\ J\ kg^{-1}\ K^{-1}$  and retaining a value of above  $10\ J\ kg^{-1}\ K^{-1}$  up to 20 K for a similar field change<sup>4,36</sup>. This gives commercially available  $HoF_3$  the potential to find uses for magnetic refrigeration over a wide temperature. The large magnetocaloric effect in these materials is partly due to the high density of the  $LnF_3$  ( $7.6441(20)\ g\ cm^{-3}$  for  $HoF_3$  at 300 K), and the large magnetic entropy of the lanthanide ions coupled with its magnetisation rapidly increasing at low applied magnetic fields.  $HoF_3$  is an extremely competitive magnetocaloric in a range of applied fields for cooling below 20 K, with potential applications including hydrogen liquefaction. The decrease of  $-\Delta S_m$  at low temperatures and the apparent inverse MCE may mean some care in its application is required but if used for cooling in the 10-20 K range this complication should be avoided. Therefore it was desirable to further explore the magnetic behaviour on a microscopic level using neutron scattering.

### C. Dynamic Magneto-structural Relationships of $HoF_3$

$Ho^{3+}$  is a non-Kramers ion, which, in combination with the low site symmetry ( $C_{1h}$ ), leads to the ground electronic state being a

non-magnetic singlet state.<sup>21,37,38</sup> It has previously been reported that a Schottky-type feature associated with transition to this ground electronic state is centred at 3.5 K but this is a broad transition and, as a result, HoF<sub>3</sub> remains paramagnetic well below 1 K.<sup>21,39</sup> HoF<sub>3</sub> magnetically order at T<sub>N</sub> = 0.53 K into a canted antiferromagnetic state, with ferromagnetic nearest neighbour correlations and strong anisotropy along the *a*-axis.<sup>39</sup> The moments have been reported to align along chain direction and canted 66° from the towards the nearest neighbour.<sup>20</sup>

Polarised inelastic neutron scattering spectra were collected on HoF<sub>3</sub> at 1.5 K as a function of *Q* and energy, and the magnetic contribution to the total spectra is shown in **FIG. 5**. The total spectra and nuclear contributions are shown in **FIG. S21-22**. This spectra did not show any indication of long range magnetic order at 1.5 K at the elastic line, consistent with the previous study. No structured magnetic diffuse scattering has been observed as has been shown in other promising Ising-spin magnetocalorics such as LnODCO<sub>3</sub> and Ln(HCO<sub>2</sub>)<sub>3</sub> phases,<sup>11,12,15-17</sup> suggesting a lack of any short range magnetic order.

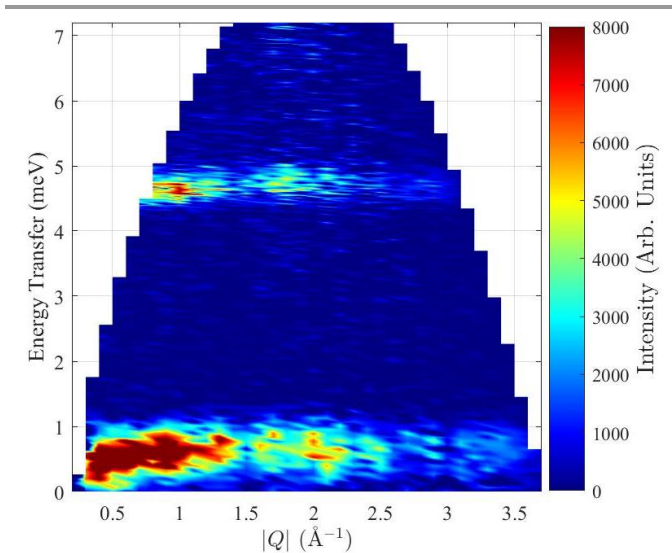


**FIG. 5:** The normalised magnetic contribution of the inelastic scattering function of HoF<sub>3</sub>, separated from the total scattering on D7 by using the XYZ polarisation analysis method. There are two clear low lying excitations centred around 0.59 meV and 4.7 meV.

Two magnetic excitations are observed in the spectra centred around ~0.59 and ~4.7 meV. These excitations relate to low lying excitations that have been previously reported to be the energy gap separating a pair of Ising-like electronic states; the ground state singlet and the excited singlet state by 5.90 cm<sup>-1</sup> (0.73 meV), and another low lying excitation at 37.99 cm<sup>-1</sup> (4.71 meV) to another excited singlet state.<sup>39,40</sup> Integration over all *Q* produces the inelastic scattering function *S*( $\omega$ ) shown in **Fig. S23**. Gaussian functions have been fit to **FIG. S23** and this finds the centre of the first excited state to be at 0.589(3) meV, lower in energy than previously reported.<sup>21,39,40</sup> The second excited state was found to be centred at 4.690(4) meV, in very good agreement with previous reports.<sup>21,40</sup> Integration along *Q* of these two excitations are shown in **FIG. 6**, which shows an increase in the inelastic scattering intensity at low *Q*, indicating these are not purely point-like transitions, as previously suggested, but are,

instead, non-localised magnetic excitations. The scattering function *S*(*Q*) of these excitations are also structured with local maxima in the scattering of both the low and high energy excitations, indicating some order to these dynamical magnetic excitations. The increase in the scattering intensity of the inelastic features with decreasing *Q*, are consistent with the presence of ferromagnetic fluctuations in the paramagnetic phase.<sup>41-43</sup>

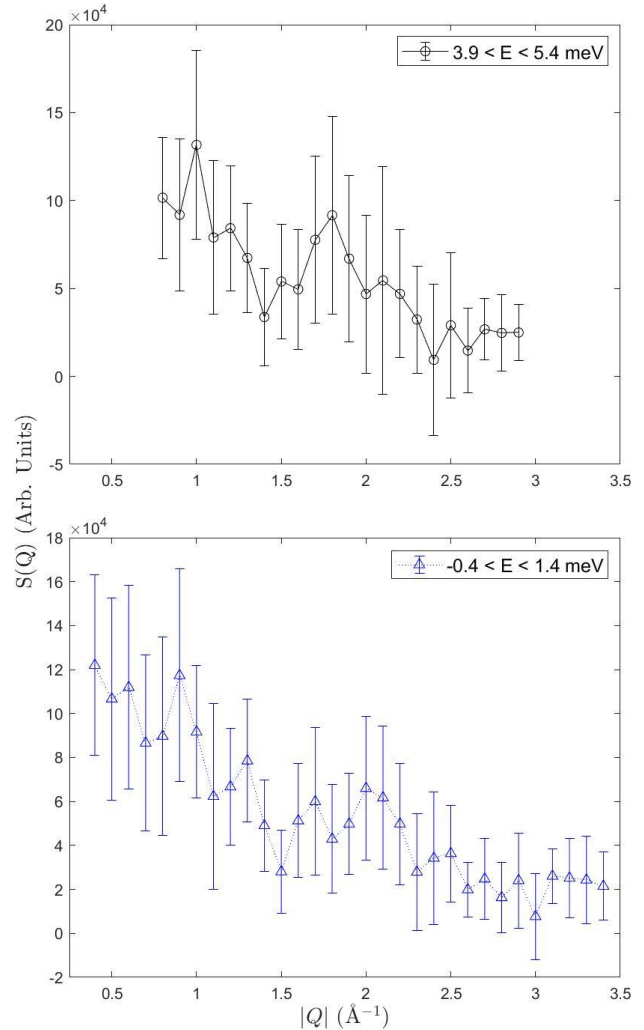


**FIG. 6:** The magnetic inelastic scattering intensity as a function of momentum transfer *S*(*Q*) of the high energy mode (top) and the low energy mode (bottom). The limits of the energy integration windows are listed in the figures.

Bleaney *et al.*<sup>21,39</sup> has previously shown a low lying state with a gap of 8.14 cm<sup>-1</sup> (1.009 meV) which has been attributed to a magnon in the magnetically ordered phase. The fit to the low energy excitation in **FIG. S23** results in a  $\delta E/E$  of ~23%, far greater than the expected energy resolution of D7 at this energy, suggesting the presence of two excitations very close in energy consistent with the previous studies suggesting two excitations at around 0.8-1.0 meV.

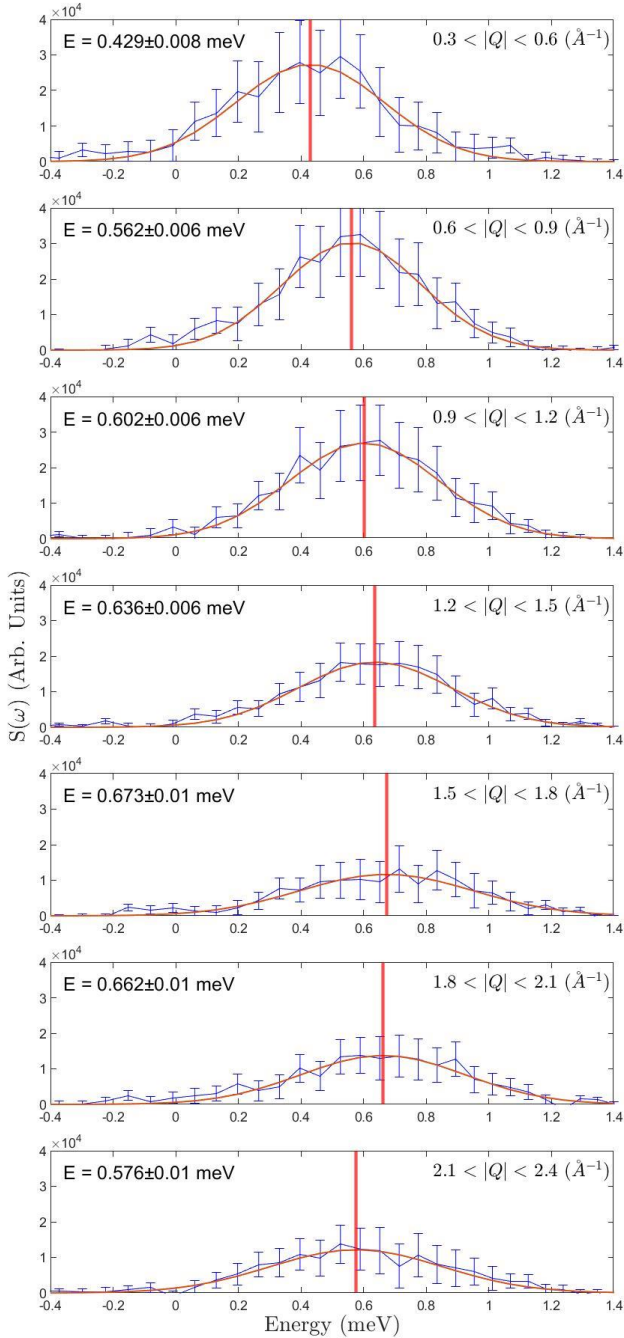


**FIG. 7:** Comparison of the energy-dependence of the magnetic inelastic scattering from the low lying excitation, at various  $Q$ . The peaks have been fitted with a Gaussian model, shown in red, to extract the peak center indicated by the vertical red line. The peak in energy changes as a function of  $Q$  indicating this mode is weakly dispersive.

To investigate the origin of the low energy magnetic feature further, the energy of the low energy excitations has been studied as a function of  $Q$ . **FIG. 7** shows the change in intensity and energy of the low energy excitation, as a function of  $Q$ . At the lowest  $Q$  bin ( $0.3 \text{ \AA}^{-1} < Q < 0.6 \text{ \AA}^{-1}$ ), the excitation is centred at  $0.429(8) \text{ meV}$ , shifting to higher energies at higher  $Q$  bins, up to  $0.636(6) \text{ meV}$  where  $1.5 \text{ \AA}^{-1} < Q < 1.8 \text{ \AA}^{-1}$ , and shifting to lower energies at the highest  $Q$  bins. The changes in energy maxima as

a function of  $Q$  is a clear indication of a dispersive excitation, providing further evidence that this excitation has a magnetic origin and is an indication of correlations in the dynamic moments in the paramagnetic phase

Therefore we would expect that at temperatures below  $T_N$ , where the temperature is no longer disrupting correlations, these features may sharpen into a well-defined spin wave. Whilst qualitatively the higher energy excitation appears to also be weakly dispersive, the statistics are quite poor and so fits are subject to a high degree of error (see **FIG. S24**).

Measurements as a function of temperature were performed in the diffraction mode of D7, without the Fermi chopper and therefore no energy analysis. The instrument integrates the scattering over all final neutron energies in this mode, and the attribution of  $Q$  is determined based on the scattering angle,  $2\theta$ , and the assumption that the scattering is quasielastic. The assumption is known as the static approximation. **FIG. 5** indicates that all of the magnetic scattering intensity in  $\text{HoF}_3$  is inelastic, with significant spectral weight in the higher energy mode, and therefore, absolute  $Q$  values using this approximation should be considered tentatively. **FIG. 8** shows the scattering intensity of  $\text{HoF}_3$  in diffraction mode integrated over all final neutron energies. The data appear to show some structure between  $1.6 < Q < 3.1 \text{ \AA}^{-1}$ , but this is due to the integration over the inelastic scattering observed in **FIG. 5** rather than any structural order. It is unlikely this structure has any significant contribution from leakage from the nuclear scattering as there is only one peak as there is limited Bragg scattering over this  $Q$ -range (*c.f.* **FIG. 5** to **FIG. S22**). Differences can be observed between lower and higher temperature polarised neutron patterns. This suggests the magnetic excitations are changing gradually with temperature. Specifically, the increase in scattering intensity at low  $Q$  indicated by inelastic spectroscopy to arise from ferromagnetic fluctuations at  $1.5 \text{ K}$  is lost above  $10 \text{ K}$ . While the dynamical spin fluctuations in  $\text{HoF}_3$  are not well described by a purely paramagnetic magnetic form factor comparison to this in **FIG. 8** does highlight this decrease in intensity on heating. It also suggests that above  $10 \text{ K}$  the magnetic scattering decreases slightly, when approaching  $Q=0$ , suggesting the presence of limited antiferromagnetic fluctuations. We interpret these observations as evidence for the existence of ferromagnetic spin fluctuations through the temperatures at which the MCE peaks in  $\text{HoF}_3$ .<sup>43</sup>

On the basis of previous studies combined with our measurements we can suggest an origin of the interesting magnetocaloric behaviour of  $\text{HoF}_3$ . The decrease of the magnetocaloric effect below  $4 \text{ K}$  and apparent significant inverse magnetocaloric effect at  $2 \text{ K}$  is likely associated with the transition to the singlet ground state, which will decrease the magnetic moment on the  $\text{Ho}^{3+}$  cation as temperature decreases. Thus the magnetisation will increase with increasing temperature as the excited states are thermally populated and the  $\text{Ho}^{3+}$  have progressively larger magnetic moment. This suggestion is supported by the temperature at which  $-\Delta S_m$  first decreases being approximately that of the heat capacity anomaly reported previously at  $3.5 \text{ K}$ .<sup>21</sup> That the remaining magnetic moments order antiferromagnetically at lower temperatures will increase

the rate at which magnetisation decreases with temperature as this approaches. Inverse MCE is not common but has been previously attributed to crystal field effects, such as in  $\text{PrNi}_5$ ,<sup>44</sup> and magnetic ordering, including in  $\text{Ba}_3\text{Tb}(\text{BO}_3)_3$  and  $\text{Dy}(\text{HCO}_2)(\text{C}_2\text{O}_4)$ ;<sup>5,45</sup> it may be both of these are relevant factors in  $\text{HoF}_3$ . With respect to the behaviour of  $\text{HoF}_3$  at higher temperature our diffuse magnetic scattering patterns of  $\text{HoF}_3$  suggest significant ferromagnetic fluctuations at 5 K, based on the known magnetic structure these are likely intrachain correlations. The close proximity of the Ho cations in  $\text{HoF}_3$  and single fluoride ion separating them, leads to the interactions between spins being quite strong with spins having strong anisotropy along the chain directions.<sup>20</sup> As for other materials with ferromagnetic chains of magnetically anisotropic spins this will enable the ready alignment of the spins under applied fields, leading to higher  $-\Delta S_m$  at low fields.<sup>11,12,15,16,18</sup> Persistence of the significant ferromagnetic intrachain interactions is likely the cause of the gradual decrease in  $-\Delta S_m$  compared to other systems in which the cations are packed less densely.

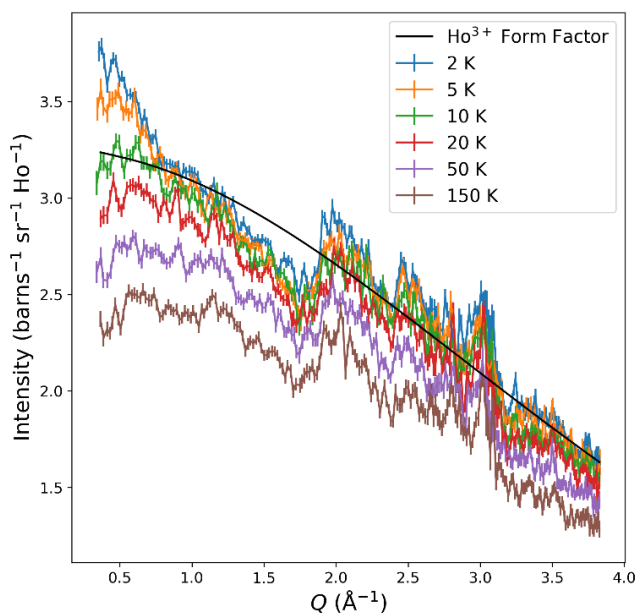


**FIG. 8:** Comparison of the magnetic scattering measured in diffraction mode, integrating over all final neutron energies, as a function of temperature between 2 and 150 K. As described in the text the scattering between  $\sim 1.6 > Q > \sim 3.1 \text{ \AA}^{-1}$  is caused by the low lying excitations and not Bragg peaks from magnetic structural order.

## Conclusions

This work has explored the magnetocaloric effects of the magnetically anisotropic  $\text{LnF}_3$  phases, which have highly competitive  $-\Delta S_m^{\text{max}}$  with respect to volume due to their dense structures. Amongst these promising materials  $\text{HoF}_3$  is the most interesting, exhibiting considerable conventional MCE above 5 K in low applied fields, which only gradually decreases with temperature such that significant magnetocaloric effects are observed up to 20 K, useful for hydrogen liquefaction. The  $-\Delta S_m$  of  $\text{HoF}_3$  decreases below 4 K with a possibility of significant inverse MCE at 2 K. Based in part on an examination of  $\text{HoF}_3$  with inelastic neutron scattering the decrease in  $-\Delta S_m$  below 4 K is attributed to the singlet ground state of  $\text{HoF}_3$  combined with

the previously reported antiferromagnetic ordering below 1 K. The promising conventional MCE at temperatures well above 10 K is attributed to the existence of significant 1D ferromagnetic correlations.

## Supplementary Materials

See supplementary material for diffraction patterns, additional magnetic properties data and further neutron spectroscopy data.

## Author Contributions

All authors contributed to this manuscript. Data collection and analysis, was primarily performed by RJCD with contributions from PWD and GBGS. This specific project was conceptualised by RJCD, and this manuscript was written by RJCD. AW contributed significantly through data collection, data reduction and supervision of neutron scattering data and analysis. PJS assisted with conceptualising the idea, acquired funding for this project, validated the analysis and contributed to the writing and editing of this manuscript.

## Conflicts of interest

There are no conflicts of interest to declare.

## Acknowledgements

RJCD would like to acknowledge the University of Kent's for financial support through the provision of a Vice-Chancellors scholarship for the initial funding. The authors would like to thank EPSRC for funding this research (EP/S03577X/1 & EP/T027886/1). We would also like to thank the Institut Laue Langevin for access to neutron scattering facilities in Grenoble. The authors would like to thank Malte Grosche and Jiasheng Chen from the Cavendish Laboratory, University of Cambridge, for useful discussions.

## References

- O. Sari and M. Balli, *Int. J. Refrig.* **37**, 8 (2014).
- A. Kitanovski, J. Tušek, U. Tomc, U. Plaznik, M. Ožbolt, and A. Poredoš, *Magnetocaloric Energy Conversion* (2015).
- T. Numazawa, K. Kamiya, T. Utaki, and K. Matsumoto, *Cryogenics* **62**, 185 (2014).
- R. Li, G. Li, and C. Greaves, *J. Mater. Chem. A* **6**, 5260 (2018).
- M. Falsaperna, G.B.G. Stenning, I. da Silva, and P.J. Saines, *J. Mater. Chem. C* **9**, 13209 (2021).
- E. Palacios, J.A. Rodríguez-Velamazán, M. Evangelisti, G.J. McIntyre, G. Lorusso, D. Visser, L.J. De Jongh, and L.A. Boatner, *Phys. Rev. B* **90**, 214423 (2014).
- Y.-Z. Zheng, G.-J. Zhou, Z. Zheng, and R.E.P. Winpenny, *Chem. Soc. Rev.* **43**, 1462 (2014).
- Y.-C. Chen, J. Prokleška, W.-J. Xu, J.-L. Liu, J. Liu, W.-X. Zhang, J.-H. Jia, V. Sechovský, and M.-L. Tong, *J. Mater. Chem. C* **3**, 12206 (2015).



- <sup>9</sup> B. Daudin, R. Lagnier, and B. Salce, *J. Magn. Magn. Mater.* **27**, 315 (1982).
- <sup>10</sup> Y. Yang, Q.C. Zhang, Y.Y. Pan, L.S. Long, and L.S. Zheng, *Chem. Commun.* **51**, 7317 (2015).
- <sup>11</sup> P.J. Saines, J.A.M. Paddison, P.M.M. Thygesen, and M.G. Tucker, *Mater. Horiz.* **2**, 528 (2015).
- <sup>12</sup> R.J.C. Dixey and P.J. Saines, *Inorg. Chem.* **57**, 12543 (2018).
- <sup>13</sup> T. Numazawa, K. Kamiya, T. Okano, and K. Matsumoto, *Phys. B Condens. Matter* **329–333**, 1656 (2003).
- <sup>14</sup> P. Mukherjee, E. Suard, and S.E. Dutton, *J. Phys. Condens. Matter* **29**, 405807 (2017).
- <sup>15</sup> R.J.C. Dixey, G.B.G. Stenning, P. Manuel, F. Orlandi, and P.J. Saines, *J. Mater. Chem. C* **7**, 13111 (2019).
- <sup>16</sup> R.J.C. Dixey, F. Orlandi, P. Manuel, P. Mukherjee, S.E. Dutton, and P.J. Saines, *Philos. Trans. R. Soc. A Math. Phys. Eng. Sci.* **377**, 20190007 (2019).
- <sup>17</sup> R.J.C. Dixey, P. Manuel, F. Orlandi, P. Mukherjee, S.E. Dutton, G.B.G. Stenning, and P.J. Saines, *J. Mater. Chem. C* **8**, 12123 (2020).
- <sup>18</sup> D.R. Harcombe, P.G. Welch, P. Manuel, P.J. Saines, and A.L. Goodwin, *Phys. Rev. B* **94**, 174429 (2016).
- <sup>19</sup> M. Piotrowski, H. Ptasiwicz-bąk, and A. Murasik, *Phys. Status Solidi* **55**, K163 (1979).
- <sup>20</sup> P.J. Brown, J.B. Forsyth, P.C. Hansen, M.J.M. Leask, R.C.C. Ward, and M.R. Wells, *J. Phys. Condens. Matter* **2**, 4471 (1990).
- <sup>21</sup> B. Bleaney, J.F. Gregg, R.W. Hill, M. Lazzouni, M.J.M. Leask, and M.R. Wells, *Le J. Phys. Colloq.* **49**, C8 (1988).
- <sup>22</sup> J. Rodríguez-Carvajal, *Phys. B Phys. Condens. Matter* **192**, 55 (1993).
- <sup>23</sup> J.R. Stewart, P.P. Deen, K.H. Andersen, H. Schober, J.-F. Barthélémy, J.M. Hillier, A.P. Murani, T. Hayes, B. Lindenau, and IUCr, *J. Appl. Crystallogr.* **42**, 69 (2009).
- <sup>24</sup> H.N. Russell and F.A. Saunders, *Astrophys. J.* **61**, 38 (1925).
- <sup>25</sup> L. Holmes and H.J. Guggenheim, *Le J. Phys. Colloq.* **32**, C1 (1971).
- <sup>26</sup> J. Brinkmann, R. Courths, S. Hüfner, and H.J. Guggenheim, *J. Magn. Magn. Mater.* **6**, 279 (1977).
- <sup>27</sup> P. Mukherjee and S.E. Dutton, *Adv. Funct. Mater.* **27**, 1701950 (2017).
- <sup>28</sup> J. Filippi, F. Tcheou, and J. Rossat-Mignod, *Solid State Commun.* **33**, 827 (1980).
- <sup>29</sup> J. Hammann and M. Ocio, *Phys. B+C* **86–88**, 1153 (1977).
- <sup>30</sup> B.L. Reid, D.F. McMorrow, P.W. Mitchell, O. Prakash, and A.P. Murani, *Phys. B Condens. Matter* **174**, 51 (1991).
- <sup>31</sup> P.J. Saines and N.C. Bristowe, *Dalt. Trans.* **47**, 13257 (2018).
- <sup>32</sup> Y. Meng, Y.-C. Chen, Z.-M. Zhang, Z.-J. Lin, and M.-L. Tong, *Inorg. Chem.* **2**, 9052 (2014).
- <sup>33</sup> Y.-C. Chen, L. Qin, Z.-S. Meng, D.-F. Yang, C. Wu, Z. Fu, Y.-Z. Zheng, J.-L. Liu, R. Tarasenko, M. Orendáč, J. Prokleška, V. Sechovský, and M.-L. Tong, *J. Mater. Chem. A* **2**, 9851 (2014).
- <sup>34</sup> H. Zhang, C. Xing, H. Zhou, X. Zheng, X. Miao, L. He, J. Chen, H. Lu, E. Liu, W. Han, H. Zhang, Y. Wang, Y. Long, L. van Eijk, and E. Brück, *Acta Mater.* **193**, 210 (2020).
- <sup>35</sup> P. Mukherjee, A.C. Sackville Hamilton, H.F.J.J. Glass, and S.E. Dutton, *J. Phys. Condens. Matter* **29**, 405808 (2017).
- <sup>36</sup> R. Li, P. Manuel, F. Orlandi, and C. Greaves, *J. Mater. Chem. A* **6**, 21149 (2018).
- <sup>37</sup> P.H.E. Meijer, *Physica* **26**, 61 (1960).
- <sup>38</sup> H. Kramers, *Physica* **1**, 182 (1934).
- <sup>39</sup> B. Bleaney, J.F. Gregg, R.W. Gregg, M. Lazzouni, M.J.M. Leask, and M.R. Wells, *J. Phys. C Solid State Phys.* **21**, 2721 (1988).
- <sup>40</sup> K.K. Sharma, F.H. Spedding, and D.R. Blinde, *Phys. Rev. B* **24**, 82 (1981).
- <sup>41</sup> Z. Huesges, M.M. Koza, J.P. Embs, T. Fennell, G. Simeoni, C. Geibel, C. Krellner, and O. Stockert, *J. Phys. Conf. Ser.* **592**, 012083 (2014).
- <sup>42</sup> S. Ramos, E.M. Forgan, C. Bowell, S.M. Hayden, A.J. Schofield, A. Wildes, E.A. Yelland, S.P. Brown, M. Laver, R.S. Perry, and Y. Maeno, *Phys. B Condens. Matter* **403**, 1270 (2008).
- <sup>43</sup> A.T. Boothroyd, R. Coldea, D.A. Tennant, D. Prabhakaran, L.M. Helme, and C.D. Frost, *Phys. Rev. Lett.* **92**, 197201 (2004).
- <sup>44</sup> P. von Ranke, V. Pecharsky, and K. Gschneidner, *Phys. Rev. B* **58**, 14436 (1998).
- <sup>45</sup> N.D. Kelly, C. Liu, and S.E. Dutton, *J. Solid State Chem.* **292**, 121640 (2020).